Progress In Electromagnetics Research B, Vol. 87, 131–149, 2020

Measurement of the Antenna Impedance Mismatch Through the Time Domain Mode of the Vector Network Analyzers: An Experimental Procedure

Angelo Gifuni[1, *], Michele Ambrosanio[1], Gabriele Gradoni [2], Giuseppe Grassini[1], Christopher Smartt[3], and Stefano Perna[1]

Abstract—In this paper we show a procedure to measure the impedance mismatch of antennas by exploiting the *Time Domain* (*TD*) *option* available in usual VNAs. The procedure can be applied even in the presence of reflecting obstacles in the measurement scenario surrounding the antenna under test (AUT).

It is shown that effective application of the procedure requires to fulfill a reduced number of constraints basically involving the distance of the AUT from the nearest obstacle, the response resolution to be set through the *TD option* of the VNA, and the length of the gating aperture to be applied to the received signal.

The proposed measurement procedure is in principle applicable to any antenna. However, it is very easy and advantageous for antennas having short responses in the time domain, such as horn antennas, where the method can likely be applied to frequencies less than 500 MHz.

Comparison between the results obtained from measurements performed inside an anechoic chamber (that is, in the absence of reflecting obstacles around the AUT), outside the anechoic chamber, and even inside a reverberation chamber, demonstrate the effectiveness of the proposed measurement procedure.

1. INTRODUCTION

Antenna impedance mismatch (AIM) is an important parameter, which coupled with the radiation efficiency, determines the total efficiency of an antenna [1, 2]. Accurate AIM measurement (AIMM) is thus of key importance for several electromagnetic applications, including those involving the use of reverberation chambers (RCs), where knowledge of the AIM allows achieving the radiation efficiency [3] and also compensating for the impedance mismatch [3–6].

Accurate AIMM is usually performed in an anechoic chamber (AC), which simulates free space, through the measurement of the reflection coefficient.

On the other hand, a cheaper, and more easy to implement, procedure alternative to the use of the AC is to give up the ideal condition of free-space, by carrying out such measurements in an electromagnetic environment where reflecting obstacles are present. To do this, time domain (TD) measurements, exploiting radiofrequency pulses as excitation, are appropriate. Indeed, to account for the possible presence of obstacles around the antenna under test (AUT), one can properly set the pulse width, in such a way that the reflections due to these obstacles can be removed through time gating [7–12]. In this regard, it is noted that in all cases a minimum distance between the AUT and the nearest

Received 1 June 2020, Accepted 9 July 2020, Scheduled 25 July 2020

* Corresponding author: Angelo Gifuni (angelo.gifuni@uniparthenope.it).

[1] Dipartimento di Ingegneria, Università di Napoli Parthenope, Centro Direzionale di Napoli, Napoli, Italy. [2] George Green Institute for Electromagnetics Research, University of Nottingham, NG7 2RD, Nottingham, UK. [3] School of Mathematical Sciences, University of Nottingham, NG7 2RD, Nottingham, UK.

obstacle must be ensured to avoid coupling effects affecting the intrinsic impedance of the AUT itself [13].

It is well known that TD measurements can be carried out by using a conventional vector network analyzer (VNA) operating in frequency domain (FD). In particular, an inverse fast Fourier transform (IFFT) is applied to obtain the corresponding TD response [14–18]; then, a gating operation and subsequent fast Fourier transform (FFT) allow obtaining the antenna reflection coefficient in FD.

In this paper we show a procedure that allows performing the AIMM in the presence of obstacles by exploiting the *TD option* available in usual VNAs.

Since the AIM is strictly connected to the reflection coefficient of an antenna [2], in the following we will refer in the same way to AIM and reflection coefficient. For this reason, in this paper results will be given in terms of reflection coefficient of the AUT.

In this regard, it is noted that knowledge of the TD response on the reflection coefficient of an antenna system is useful for very short range radar systems, such as some ground penetrating radar (GPR) [19, 20], for through the wall radar (TWR) [21], and for distinguishing direct wave from the reflected wave in several problems [13, 22, 23]. Hence, in a wide range of application contexts, the use of the gating operation is well known and extensively applied. However, to the best of our knowledge, the systematic description of the measurement procedure that allows obtaining the AIM in any electromagnetic environment (particularly, in the presence of obstacles), by exploiting the *TD option* available in usual VNAs is not explicitly present in literature. For instance, in [24], the application to a single case of double ridge horn antenna is shown, where however a different measurement strategy is adopted, and the *TD option* available in usual VNAs is not exploited.

The measurement procedure described in this work has been applied to some common antennas; its effectiveness is proved by comparing the obtained measurement results and those achieved in an AC. Moreover, to show the effectiveness of the proposed procedure, we have applied it even in an RC, which, in contrast to the AC, represents a measurement environment characterized by several obstacles.

2. MEASUREMENT PROCEDURE: CONSTRAINTS ON SETTINGS

This Section provides the description and analysis of the constraints on settings to be enforced in order to measure the AIM in the presence of obstacles by exploiting the *TD option* available in usual VNAs. As clarified above, such a measurement procedure is based on the cascade of the following main steps:

- application of the IFFT to the signal measured by the VNA in FD;
- application of the gating operation;
- application of the FFT to obtain the antenna reflection coefficient in FD.

All these steps can be carried out through the *TD option* embedded in the VNA [14–18], which also allows the application of possible signal compensation procedures [14–18]. Windowing aspects on the IFFT and gating shape related to the FFT [7–12] can be conveniently selected in the *TD option* as well.

In our case, no compensation concerning the amplitude is necessary for the attenuation of the signal, since the reference plane of the AUT is connected at the measurement calibration plane. This means that no reflection occurs before the reference plane of the AUT.

Some considerations relevant to the appropriate selection of the gating aperture (GA) are now in order.

First of all, it is important to note that the GA should include the whole reflection response interval of the AUT. In this regard, it is worth noting that each antenna has its own specific reflection response interval, which depends on the physical structure and on the frequency range (FR) of the antenna itself. As an example, it is seen that the reflection response interval of double ridge waveguide horn antennas is shorter than that of the log-periodic antennas. The latter are fed from the tip by a coaxial cable that connects the reference plane and the tip of the antenna, along with a balun. Non-negligible multiple reflections can be excited along the body of such antennas; i.e., a pattern of stationary waves can be present along the body of such antennas. These multiple reflections, which are non-negligible at the lower frequencies of the antenna bandwidth, produce an enlargement of the reflection response interval with respect to that observed at higher frequencies. It is likely that this phenomenon exists for horn and double ridge waveguide horn antennas as well, but in these cases it is negligible, even when such

antennas work in the lower region of their bandwidth, that is, at 200 MHz. For the specifications on such antennas, see as an example [25, 26]. In fact, for double ridge waveguide horn antennas, the reflection from the mouth of the antennas is very weak and does not excite non-negligible multiple reflections along the body of such antennas.

In summary, to achieve accurate AIMM, it must be taken into account that the reflection response interval depends on the AUT itself and the operating frequency adopted during the measurement procedure.

For the sake of clearness, hereafter in the paper, the following assumptions are made:

- c is the light speed in free space;
- the operational FR of the AUT is $[f_{\mathrm{MIN}},\ f_{MAX}]$; the corresponding wavelength spans from λ_{MAX} to λ_{MIN};
- the reference time is denoted by $t_0 = 0$, which converted in space corresponds to the calibration plane;
- the AUT reflection response is a time interval that ranges from $t_{\mathrm{AUT}}^{\mathrm{beg}}$ to $t_{\mathrm{AUT}}^{\mathrm{end}}$;
- the distance between the physical structure of the AUT and the nearest obstacle (in any direction where the reflection is appreciable) is equal to d, which is adjustable for a given measurement setup by moving the obstacle itself; such a distance is also called nearest-obstacle distance in this paper;
- the reflection response due to the nearest obstacle start at $t_{\mathrm{obs}}^{\mathrm{beg}}$, where the subscript obs mean obstacle;
- the response resolution (in time) that can be set through the *TD option* of the VNA is denoted as T_{res} and corresponds to the 50% of the pulse width when bandpass mode and normal windowing are selected in the *TD option* [16] (as in all the measurements presented in this paper), we have that $T_{res} \sim 2/\Delta f$ [16], being Δf the frequency range chosen for the VNA measurement.

As shown below, it can be convenient to set Δf in such a way to strictly include the operational FR of the AUT.

To achieve accurate AIMM by exploiting the *TD option* available in usual VNAs, the following two constraints need to be satisfied.

Constraint 1: $d > \lambda_{\mathrm{MAX}}$

This condition guarantees that all the obstacles present in the measurement scenario do not fall inside the near field region of the AUT. For the purposes of this paper, the effect of the near field region on the AIM for a linear antenna can certainly be considered negligible if this constraint is satisfied. This is experimentally observed in the measurements performed for this paper, confirming the theory presented in [1, 2].

At least in principle, one can think to replace this condition by substituting λ_{MAX} with the maximum wavelength of the frequency range Δf chosen for the VNA measurement.

Constraint 2: $t_{\mathrm{obs}}^{\mathrm{beg}} - t_{\mathrm{AUT}}^{\mathrm{end}} \geq T_{res}$

This condition guarantees a safety margin on the separation between the antenna reflection response and the contribution provided by the nearest obstacle to the AUT.

If these two constraints are satisfied, the GA, say $[t_{\mathrm{GA}}^{\mathrm{beg}},\ t_{\mathrm{GA}}^{\mathrm{end}}]$, should be set according to the following condition:

$$\begin{aligned} t_{\mathrm{GA}}^{\mathrm{beg}} &= t_{\mathrm{AUT}}^{\mathrm{beg}} - \frac{T_{res}}{2} \\ t_{\mathrm{GA}}^{\mathrm{end}} &= t_{\mathrm{AUT}}^{\mathrm{end}} + \frac{T_{res}}{2} \end{aligned} \tag{1}$$

Note that $t_{\mathrm{AUT}}^{\mathrm{beg}}$, $t_{\mathrm{AUT}}^{\mathrm{end}}$ and $t_{\mathrm{obs}}^{\mathrm{beg}}$ are easily found in TD trace provided that T_{res} satisfies the constraint 2. Nevertheless, mathematical criteria could be thought for such an estimation.

Summing up, if the two aforementioned constrains are satisfied, and the GA is set according to the condition in Eq. (1), the AUT reflection response and the contribution provided by the nearest

obstacle will be separately visible in TD. It is recalled that although the measurements are performed by the VNA in FD, the TD trace is straightforwardly obtained through the embedded *TD option* of the instrument.

Some further considerations are in order.

When the end of the AUT reflection response is not clearly visible in the TD trace, one can think to profitably exploit a predominant reflecting obstacle properly placed around the AUT. Indeed, a predominant reflecting obstacle can be placed within the radiation pattern of the AUT, preferably, along the direction of maximum radiation, in such a way that it is closer than any other reflecting obstacle to the AUT. This allows a clear separation of the AUT reflection response from all the reflections of the environment. Note however that the two constraints listed above (particularly Constraint 2) need to be enforced when placing this predominant reflecting obstacle. To do this, one can easily measure in the TD trace the temporal delay associated to this predominant reflecting obstacle, with the aim of iteratively adjusting during subsequent trial measurements the position of the obstacle itself. This iterative process can be stopped when the reflection of the obstacle is clearly separated from the AUT reflection response. At this stage, the final test can be recorded.

In the following sections, measurements of the reflection response of some testing antennas are performed in an AC to corroborate the described procedure.

3. MEASUREMENTS

Measurements of the S_{11} coefficient of AUTs are considered. They are acquired in a full AC [27], outside the AC, and in an RC [28–30]. Five different antennas were used for the measurements: an X-Band standard horn antenna, an X-Band flanged standard waveguide antenna, a double ridge waveguide horn antenna, a log-periodic antenna, and a sleeve monopole antenna, which are shown in Fig. 1.

The S_{11} coefficient is measured by a two-port VNA, Agilent model 8363B, which is connected to the AUT by a waveguide or a coaxial cable or their combination for the cases of the X-Band standard horn antenna and of the X-Band flanged standard waveguide antenna. However, at the antenna reference plane, which is the plane where an antenna is fed, the X-Band flanged standard waveguide has to be used for the X-Band standard horn antenna and X-Band flanged standard waveguide antenna. Note that the X-Band flanged standard waveguide is the X-Band flanged standard waveguide antenna. The X-Band FR is from 8.2 GHz to 12.4 GHz and that the flanges of the waveguide used in measurements are rectangular. The standard horn antenna is a Narda, model 640. The double ridge waveguide horn antenna is an ETS-Lindgren 3115; its FR is from 1 GHz to 18 GHz. The log-periodic antenna is a Schwarzbeck Mess-Elektronik, model USLP 9143; its usable FR is from 250 MHz to 8 GHz for EMC tests. The monopole antenna is a homemade sleeve monopole, which is equipped with a ground plane of size 12 cm × 12 cm as shown in Fig. 1(g) and in Fig. 1(h); it is tested in the FR from 1 GHz to 18 GHz. For a short description of the homemade sleeve monopole, see Appendix A.

At the calibration plane, which coincides with the reference plane of the AUT, a one-port reflection calibration is made. Results and comparisons are shown below in order to validate the practical application of the proposed method.

The AC used for measurements is a full rectangular anechoic chamber of 72 m^3 volume, whose size is 3 m × 3 m × 8 m; an inside view of this AC is shown in Fig. 1(a). The performance of this AC is high above 1 GHz but decreases with decreasing frequency. However, tests made for the log-periodic antenna at frequency lower than 1 GHz can be considered acceptable for measurements type in this paper. Note that $\lambda_{\max,FR}$ for the log-periodic antenna is 1.2 m.

Two RCs are used for the measurements reported in this paper: one smaller than the other. The smaller RC is a rectangular chamber of 8 m^3 volume, whose size is 2 m × 2 m × 2 m. The input electromagnetic field can be randomized by means of three stirrers that work only in continuous mode. It is required that all stirrers are stopped during the acquisition of measurements. An inside view of this RC is shown in Fig. 1(e), Fig. 1(f), and Fig. 1(h). In this chamber, the reflection coefficient of the horn standard antenna, flanged standard antenna, double ridge waveguide horn antenna and homemade monopole antenna are measured.

The larger RC is a rectangular chamber of 120 m^3 volume, whose size is 6 m × 5 m × 4 m. The input electromagnetic field can be randomized by means of five metallic stirrers: two of them can work both

in step mode and in continuous mode whereas three of them work only in continuous mode. However, it is required that all stirrers are stopped during the acquisition of the measurements in this work. An inside view of this RC is shown in Fig. 1(i). In this chamber, the reflection coefficient of the log-periodic antenna is measured.

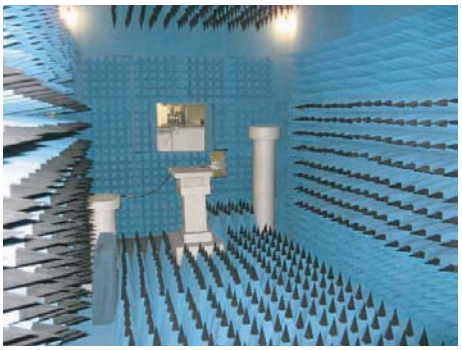

(a)

(b)

(c)

(d)

(e)

(f)

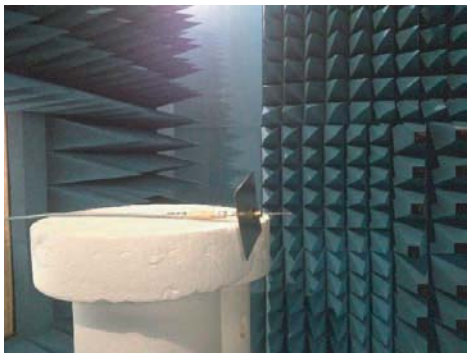

(g)

(h)

(i) (j)

Figure 1. (a) Inside view of the AC. (b) Standard horn antenna outside the AC: a metallic slab is located in front of the antenna at a distance of about 30 cm. (c) Standard horn antenna outside the AC: multiple reflecting obstacles are located in front of the antenna at different distances. (d) Double ridge waveguide horn antenna outside the AC: multiple reflecting obstacles are located in front of the antenna at different distances. (e) Standard horn antenna inside the smaller RC. (f) Double ridge waveguide horn antenna inside the smaller RC. (g) Sleeve monopole equipped with a ground plane inside the AC. (h) Sleeve monopole equipped with a ground plane inside the smaller RC. (i) Log-periodic antenna inside the larger RC. (j) Log-periodic antenna outside the AC.

In short, the two RCs are complex cavities in the presence of the associated stirrers. For measurements performed outside the AC, several configurations were used. In most cases, both a single metallic obstacle and multiple metallic obstacles were put in the main half-space for the radiation of the AUT. From Fig. 1(a) to Fig. 1(j) some configurations of the antennas in the environments of tests are shown.

The settings for the measurements of S_{11} are the FR and step frequency (SF), which determine the resolution (in TD) and the range (in TD), respectively. Different settings may be used for the different measurement setups and according to the AUT. From this point of view, measurements could be optimized. In fact, for measurements performed in AC, the necessary range is minimum as the environment simulates free space whereas for measurements performed outer the AC and a fortiori inside the RCs, the necessary range has to be increased so that the GA does not include any part including appreciable faraway scatterers or any non-negligible TD response due to multipath. These issues will be clarified in the following discussions.

However, the optimization of the settings of these measurements is not strictly necessary when the performance of the acquisition and data processing systems are performing well, so that a smaller SF than that strictly required could be used as in some cases in this paper. This corresponds to the use of a number of frequency samples greater than that strictly required. An intermediate frequency bandwidth (IFBW) of 1 kHz and a source power of -17 dBm was used in all measurements performed for the results shown in this paper. These two settings are important for the measurement uncertainty (MU). Note that the AUT was located on a polyester support for the measurements. The heights of such supports, as well as the nearest-obstacle distance, was 95 cm for the X-Band standard horn antenna, flanged standard waveguide antenna, and for double ridge waveguide horn antenna; 60 cm for sleeve monopole antenna, and 160 cm for log-periodic antenna, except where a different nearest-obstacle distance is specified, as for cases where one or more reflecting metallic slabs are used. In practise, such a distance, which corresponds to d, can also be gradually adjusted according to the measured AUT reflection response as above mentioned. In any case, it was chosen so that Eq. (1), as well as any necessary constraint, was applied correctly.

Note that the measurement frequency range Δf and number of samples, i.e., the SF, are specifically chosen so that a sufficient TD resolution, as well as a convenient measurement time range, is obtained. Although Δf is usually set equal to the AUT FR, we show in the following that it may be convenient to slightly enlarge Δf, so that it strictly includes the AUT FR. This enhances the proposed technique as it tends to remove the effects of the truncated frequency according to the enlargement of Δf with

respect to the AUT FR. For instance, for the X-Band standard horn antenna and flanged standard waveguide, we have set $\Delta f = [7\,\text{GHz}, 13\,\text{GHz}]$ in the measurements performed inside the AC, outside it, and inside the RC. We have thus selected Δf wider than the above reported FR of the antennas. The number of samples was 3001, 6001, and 16001 for measurements performed inside the AC, outside it, and inside the RC, respectively. Moreover, for measurements performed inside the RC, an FR from 8 GHz to 12.5 GHz was also used in order to verify the usefulness of the extension of the measurement FR.

It is noted that the reflection coefficient measured outside the FR of the AUT may not be connected to the concept of impedance. This occurs at frequencies greater than f_{MAX} for AUTs having a coaxial connector at reference plane, if higher order modes are excited as well, and at frequencies smaller than f_{MIN} and greater than f_{MAX} for AUTs having a waveguide at reference plane. For similar reasons, the values of the reflection coefficient measured outside the FR of the AUT may turn out to be unexpected due to the calibration procedure (that is also performed outside the FR of the guidance structure). All that does not invalidate the abovementioned enhancement of the measurement technique as the involved mathematical processes for the calculation of AIMM are not invalid, except cases where sudden variations are present in the FD measurement results.

For the double ridge waveguide horn antenna, an FR from 100 MHz to 20 GHz was used in the measurements performed inside the AC, outside it, and inside the RC. The number of samples was set to be 9901, 16001, and 16001 for measurements performed inside the AC, outside it, and inside the RC, respectively. Moreover, for measurements performed inside the RC, an FR from 1 GHz to 18 GHz was also used in order to verify the usefulness of the extension of the measurement FR.

For the sleeve monopole antenna, an FR from 100 MHz to 20 GHz was used in the measurements performed inside the AC, outside it, and inside the RC; with the number of samples set to 16001, 16001, and 16001 for measurements performed inside the AC, outside it, and inside the RC, respectively.

For the log-periodic antenna, an FR from 100 MHz to 9 GHz was used in the measurements performed inside the AC, outside it, and inside the RC; and a sample number of 4451, 16001, and 16001 was set for measurements performed inside the AC, outside it, and inside the RC, respectively. Moreover, for measurements performed inside the RC, an FR from 250 MHz to 9 GHz was also used in order to verify the usefulness of the extension of the measurement FR (only at low frequencies in this case).

The MU of the reflection coefficient, which can be found on the data sheet of the VNA used in measurements, depends on the IFBW, source power, FR of the measure, and on the amplitude of the measured coefficient, respectively.

4. RESULTS

Figure 2(a) shows the mismatch (S_{11}) in dB of the X-Band flanged standard waveguide antenna measured in the AC and outside the AC; in the latter case, a metallic slab was put in front of the antenna at a distance of about 30 cm. Fig. 2(b) shows the corresponding mismatch in TD, where the response of the AUT and that the metallic slab are clearly visible. It can be noted that the correct GA, which ranges from -1.5 ns to 1.5 ns, can be achieved both by measurements inside and outside the AC. It can also be noted that mismatch by gating from measurements outside the AC and the mismatch from measurements inside AC agree very well over the entire FR of the AUT.

Figures 3(a) and 3(b) show results from measurements performed in the smaller RC. Measurements performed in the AC are also shown. We still note that the correct GA can be even achieved by measurements inside the RC for such an antenna. We also note that mismatch by gating from measurements inside the RC agrees very well with the mismatch from measurements in AC in the FR of the AUT.

Figure 4 shows the same measurements as in Fig. 3(a) except for the FR of the measurements performed in the smaller RC, which ranges from 8.2 to 12.4 GHz. We note that in this case the mismatch by gating still agrees very well with the mismatch from measurements in the AC including at the edges of the trace. It is likely that this is why the variable part of the reflection coefficient is smaller than the constant part. The latter represents the intrinsic mismatch of the AUT.

The time reflection responses (S_{11} in TD) shown in Figs. 2 to 14 are exactly as they were displayed

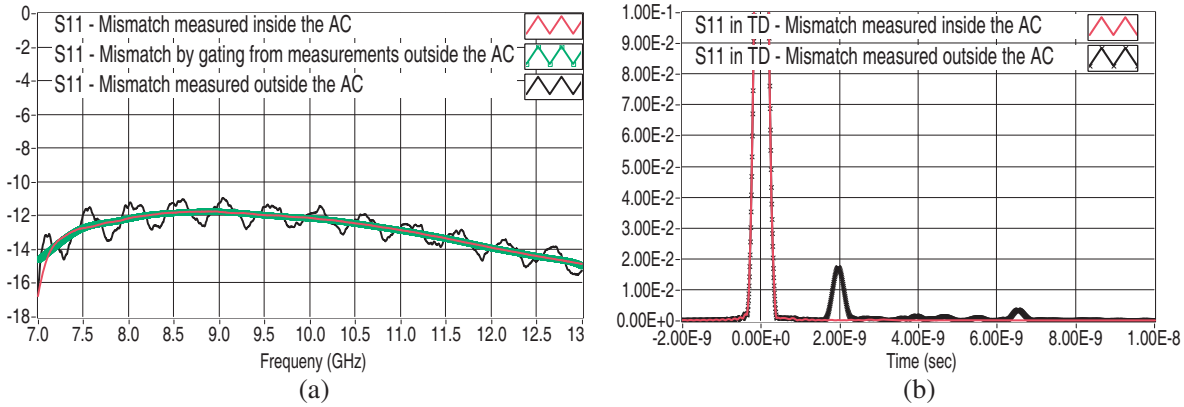

Figure 2. (a) Mismatch (S_{11}) in dB of the X-Band flanged standard waveguide antenna. Red and unmarked trace is the measurement inside the AC. Black and unmarked trace is the measurement outside the AC, where a metallic slab is in front of the antenna at a distance of about 30 cm. Green and square-marked trace is the mismatch by gating from measurements outside the AC. The GA ranges from -1.5 ns to 1.5 ns. In order to avoid misunderstandings, it is stressed that the part of measurements outside the FR of the AUT does not correspond to any modal impedance. (b) Mismatch (S_{11} in TD) of the X-Band flanged standard waveguide antenna in TD. Red and unmarked trace is the TD response concerning S_{11} inside the AC. Black and cross-marked trace is the TD response concerning S_{11} outside the AC where a metallic slab is in front of the antenna at a distance of about 30 cm.

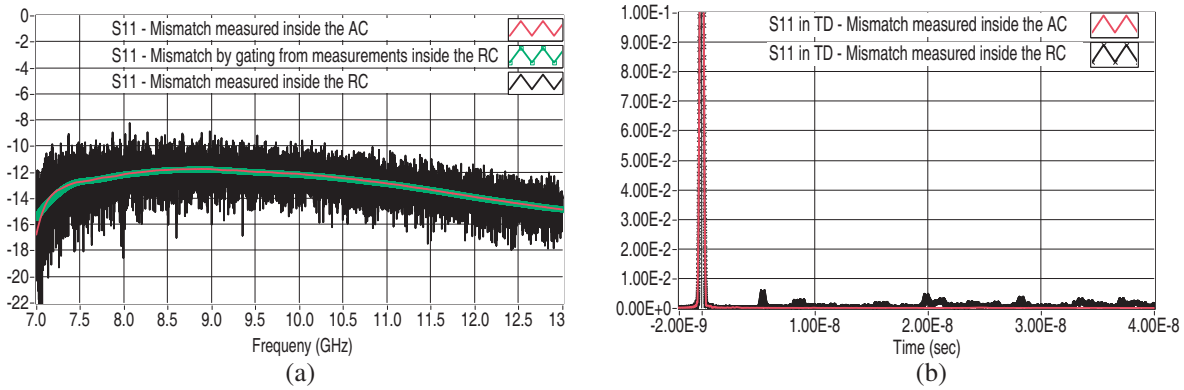

Figure 3. (a) Mismatch (S_{11}) in dB of the X-Band flanged standard waveguide antenna. Red and unmarked trace is the measurement inside the AC. Black and unmarked trace is the measurement inside the RC. Green and square-marked trace is the mismatch by gating from measurements inside the RC. The GA ranges from -1.5 ns to 1.5 ns. In order to avoid misunderstandings, it is stressed that the part of measurements outside the FR of the AUT does not correspond to any modal impedance. (b) Mismatch (S_{11} in TD) of the X-Band flanged standard waveguide antenna in TD. Red and unmarked trace is the TD response concerning S_{11} inside the AC. Black and cross-marked trace is the TD response concerning S_{11} inside the RC; the antenna was pointed toward a wall with no stirrer at a distance of about 75 cm.

and saved by the VNA with the time ranges and scales as selected, except for the TD traces in the Fig. 7(b), Fig. 15(c), Figs. 17(a), and 17(b), which were achieved by off-line data processing. In these cases, the traces were not saved to file from the TD option embedded in the VNA. The traces from VNA were stored so that they include the effects of the windowing, which was set in "bandpass mode" and was achieved by applying a Kiser-Bessel window, where the selected coefficient β was equal to 6 (the Kiser-Bessel window is available in TD option embedded in the VNA and its form can be changed by selecting the β value). The gating shape was set in "normal". These effects are without prejudice

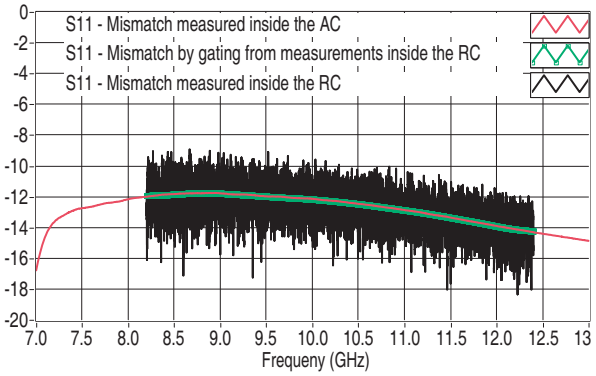

Figure 4. Mismatch (S_{11}) of the X-Band flanged standard waveguide antenna. Red and unmarked trace is the measurement inside the AC. Black and unmarked trace is the measurement inside the RC. Green and square-marked trace is the mismatch by gating from measurements inside the RC. The GA ranges from −1.5 ns to 1.5 ns. In order to avoid misunderstandings, it is stressed that the part of measurements outside the FR of the AUT does not correspond to any modal impedance.

on the selected gate aperture in cases of the Figs from 2 to 13, as shown in the results. The coefficient β of the window is given when it is different from 6 in cases of the TD traces achieved by off-line data processing.

In the cases of Figs. 15(c), 16(c), and 17(a), which concern the log-periodic antenna, the effects of the windowing spoil an easy read of the gate aperture. This fact is particularly observed in Fig. 17(b) where the coefficient β of the Kiser-Bessel window was put to zero. However, it was noted that the reflection response is long enough to limit the use of the method at low frequencies for this antenna. The length of the reflection response of such an antenna is due to the standing wave excited along the body of the antenna itself as mentioned above. These results are shown in Figs. 17(a) and 17(b) along with the possible increase of the reflection response of the AUT when the extension of the FR is applied; this is also discussed below.

It is important to note that no contribution from multipath inside the smaller RC is present in the GA as Fig. 3(b) shows. It means that the SF used was correct.

Results from Fig. 5 to Fig. 9 concern the X-band standard horn antenna. Results from several configurations are shown. These follow the same rationale of the previous results and measurements. In Fig. 5(b), the response of the metallic slab located in front of the antenna at a distance of about 40 cm is clearly visible and separated from the AUT reflection response. In all traces in TD of from Figs. 5 to 9, the throat and the mouth of the AUT are well visible. In all cases, the length of the AUT reflection response is easily separable by gating, whose aperture can easily be read from the TD traces; the GA used for such Figs. ranges from −2 ns to 2 ns.

Results in Fig. 7 concern a configuration where no reflecting obstacle was included in the environment. Fig. 9(a) shows the effect of truncation; this is overcome in Fig. 8(a) by the extension of the measurement FR; in both cases, the reflection from the RC wall where the antenna is pointed is well visible.

It can still be noted that mismatch by gating from the measurements outside the AC and inside the RC agrees very well with the mismatch from measurements inside AC over the entire FR of the AUT.

Now, it is clear that for measurements performed outside the AC or inside the RC, the range has to be increased so that the GA from the side of negative time does not include any part concerning appreciable faraway targets or any non-negligible TD response due to multipath.

Results from Fig. 10 to Fig. 12 concern the double ridge waveguide horn antenna. Measurements were performed inside the AC, outside the AC, and inside the smaller RC. Note that also for such a horn antenna, the mouth of the antenna is visible, and in all cases the length of the AUT reflection response is easily detachable by gating, whose aperture can easily be read from the TD traces. The GA used for these figures ranges from −2 ns to 2 ns. Fig. 12 shows that the effects of truncation are

entirely negligible in this case. It can still be noted that the mismatch obtained by gating from the measurements outside the AC and inside the RC agrees very well with the mismatch from measurements inside AC.

Note that the nearest-obstacle distance (d) starts from the mouth of the AUT for horn antennas.

Results from Fig. 13 to Fig. 14 concern the homemade sleeve monopole antenna. Measurements were performed inside the AC, outside the AC, and inside the smaller RC. Note that in all cases the length of the reflection response of the AUT is well detachable by gating, whose aperture can easily be read by the TD traces. The GA used for such figures ranges from -2 ns to 4 ns. In Fig. 14, it can be noted that the mismatch by gating from the measurements inside the RC agrees very well with the mismatch from measurements in AC.

In Fig. 13, it is also important to note that no significant difference is noted between results from measurements performed inside the AC and those performed outside of it. It is likely due to the radiation pattern of the AUT and to the distance of the reflecting obstacles in the measurement configuration. Even though gating is not strictly necessary in this case, these results are shown as well.

Results from Fig. 15(a) to Fig. 17(b) concern the log-periodic antenna. In particular, Fig. 15 shows results from measurements performed inside the AC and outside the AC; Fig. 16 shows results from measurements performed inside the AC and inside the larger RC; Fig. 17(a) and Fig. 17(b) show TD traces in order to highlight possible effects of the windowing and of the extension of the measurement FR on the easy identification of the length of the AUT reflection response. In particular, Fig. 15(b) shows some details at low frequency of Fig. 15(a). Fig. 15(c) shows some details of the TD responses. Similarly, Fig. 16(b) shows details at low frequency of Fig. 16(a). Fig. 16(c) shows some details of the TD responses. By results from measurements inside the AC, outside AC, and even inside the larger RC, we could measure the length of the AUT reflection response in this case as well. In this case, the nearest-obstacle distance (d) around the AUT starts from the mismatch at the tip of the antenna until the trace finally reaches a low enough level, including the whole AUT reflection response. For reasons of practicability of the method, we used a GA from -4 ns to 15 ns.

Note that the proposed method is not particularly useful for the measurement of the reflection coefficient of the log-periodic antenna performed in the configuration outside the AC, which includes the nearest-obstacle distance. It is even problematic for frequencies less than 700 MHz. However, we show the results for such configurations as well. We stress that when a reflecting obstacle is put along the direction of maximum radiation, the mismatch is strongly affected. It is found that when a metallic

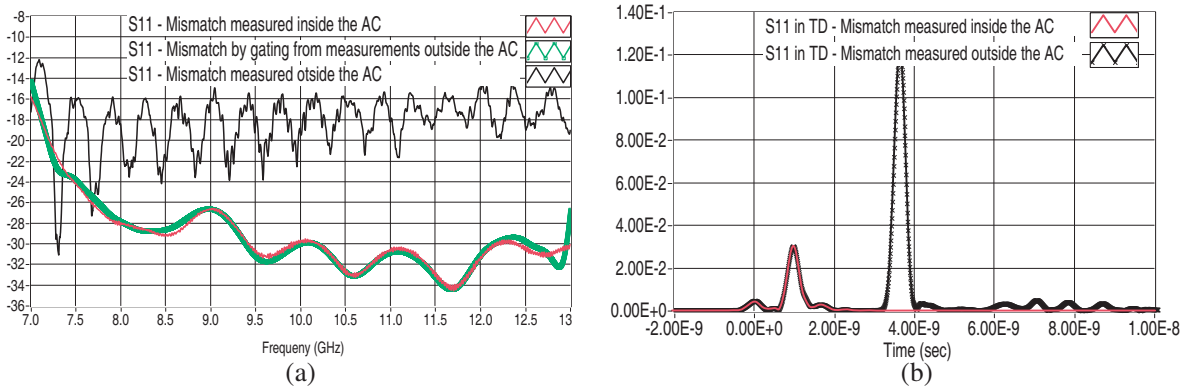

Figure 5. (a) Mismatch (S_{11}) in dB of the X-Band standard horn antenna. Red and unmarked trace is the measurement inside the AC. Black and unmarked trace is the measurement outside the AC where a metallic slab is in front of the antenna at a distance of about 40 cm. Green and square-marked trace is the mismatch by gating from measurements outside the AC. The GA ranges from -2 ns to 2 ns. In order to avoid misunderstandings, it is stressed that the part of measurements outside the FR of the AUT does not correspond to any modal impedance. (b) Mismatch (S_{11} in TD) of the X-Band standard horn antenna in TD. Red and unmarked trace is the TD response concerning S_{11} inside the AC. Black and cross-marked trace is the TD response concerning S_{11} outside the AC where a metallic slab is in front of the antenna at a distance of about 40 cm.

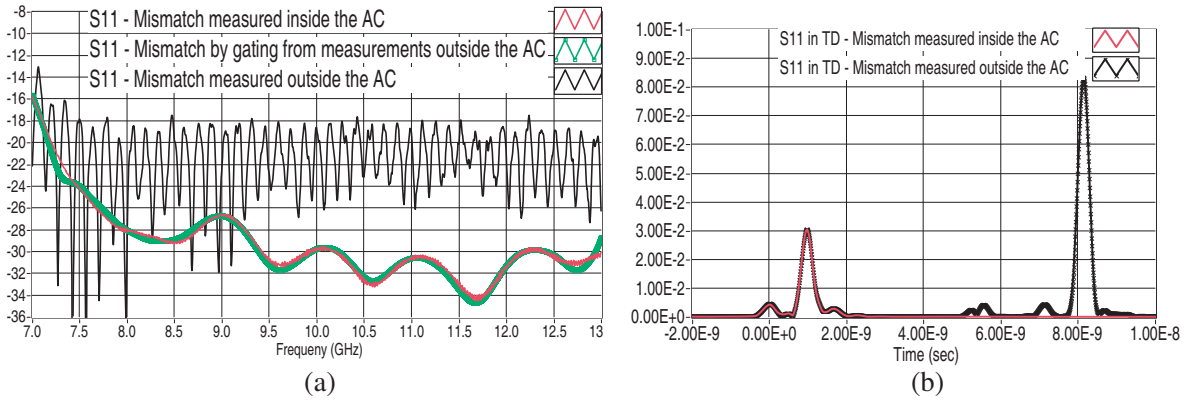

(a) (b)

Figure 6. Mismatch (S_{11}) in dB of the X-Band standard horn antenna. Red and unmarked trace is the measurement inside the AC. Black and unmarked trace is the measurement outside the AC where several metallic slabs were around the AUT at different distances and where the reflection of one of them is predominant. Green and square-marked trace is the mismatch by gating from measurements outside the AC. The GA ranges from -2 ns to 2 ns. In order to avoid misunderstandings, it is stressed that the part of measurements outside the FR of the AUT does not correspond to any modal impedance. (b) Mismatch (S_{11} in TD) of the X-Band standard horn antenna in TD. Red and unmarked trace is the TD response concerning S_{11} inside the AC. Black and cross-marked trace is the TD response concerning S_{11} outside the AC where several metallic obstacles were present around the AUT whose one was dominant.

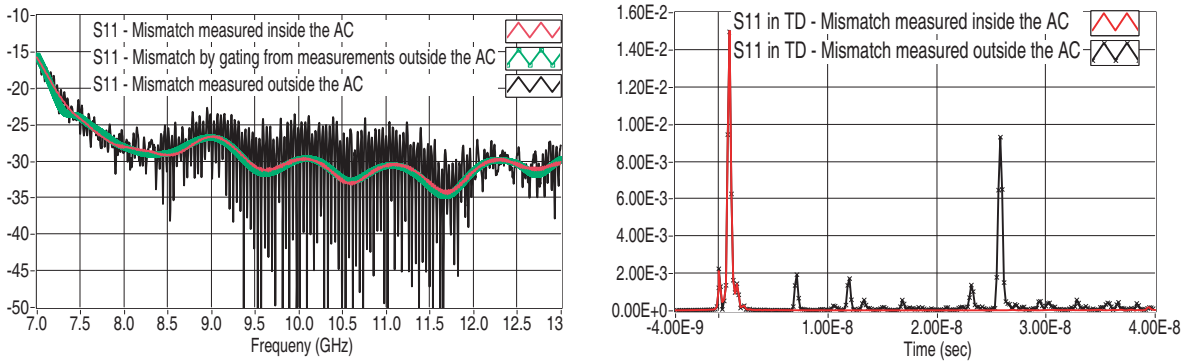

(a) (b)

Figure 7. Mismatch (S_{11}) in dB of the X-Band standard horn antenna. Red and unmarked trace is the measurement inside the AC. Black and unmarked trace is the measurement outside the AC where only the obstacles in the environment were present around the AUT (that is, no predominant reflecting obstacle was added around the AUT); the minimum distance of such obstacles was greater than 40 cm. Green and square-marked trace is the mismatch by gating from measurements outside the AC. The GA ranges from -2 ns to 2 ns. In order to avoid misunderstandings, it is stressed that the part of measurements outside the FR of the AUT does not correspond to any modal impedance. (b) Mismatch (S_{11} in TD) of the X-Band standard horn antenna in TD obtained by off-line data processing. Red and unmarked trace is the TD response concerning S_{11} inside the AC. Black and cross-marked trace is the TD response concerning S_{11} outside the AC where only the obstacles in the environment were present around the AUT; the minimum distance of such obstacles was greater than 40 cm.

slab is put orthogonally to the maximum direction of radiation and parallel to the dipoles of the AUT, results from gating are equal to those in Figs. 15 and 16 up to $d = 60$ cm, if the FR of the AUT is considered.

It is noted that the TD traces in Fig. 15(c), Figs. 17(a), and 17(b) were achieved by off-line data processing.

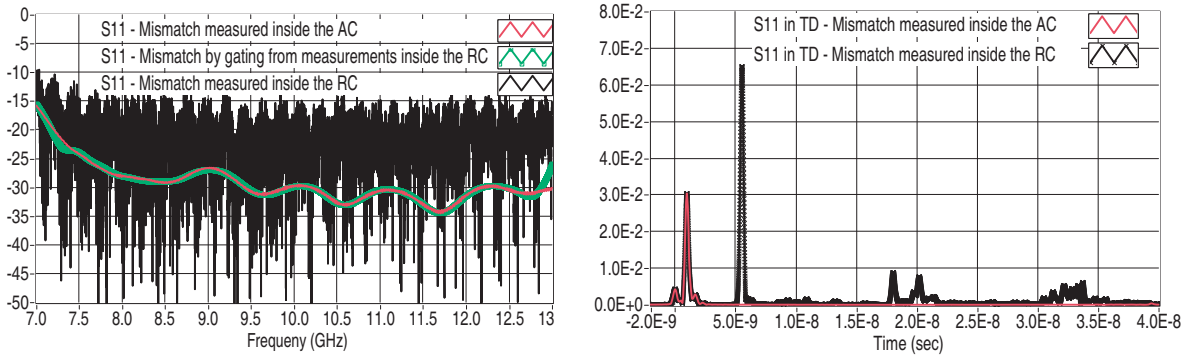

(a) (b)

Figure 8. Mismatch (S_{11}) in dB of the X-Band standard horn antenna. Red and unmarked trace is the measurement inside the AC. Black and unmarked trace is the measurement inside the RC, where the antenna was pointed toward a wall with no stirrer at a distance of about 75 cm. Green and square-marked trace is the mismatch by gating from measurements inside the RC. The GA ranges from −2 ns to 2 ns. In order to avoid misunderstandings, it is stressed that the part of measurements outside the FR of the AUT does not correspond to any modal impedance. (b) TD. Mismatch (S_{11} in TD) of the X-Band standard horn antenna in TD. Red and unmarked trace is the TD response concerning S_{11} inside the AC. Black and cross-marked trace is the TD response concerning S_{11} inside the RC; the antenna was obliquely pointed toward a wall with no stirrer at a distance of about 75 cm.

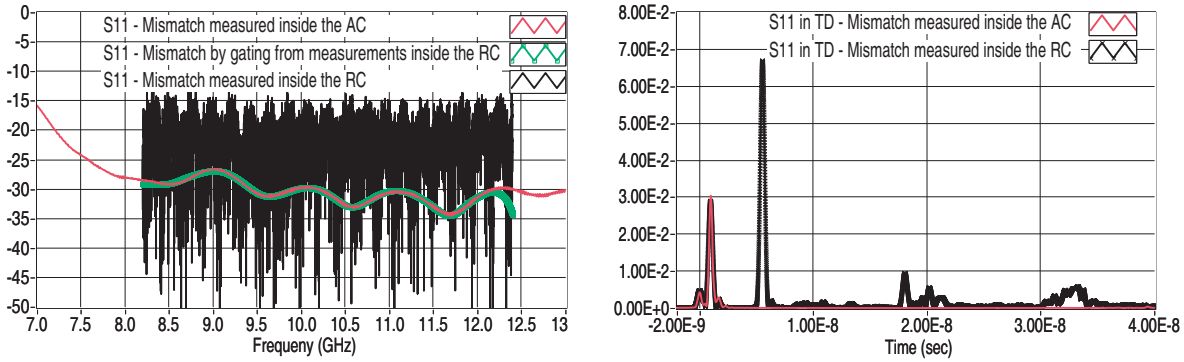

(a) (b)

Figure 9. Mismatch (S_{11}) in dB of the X-Band standard horn antenna. Red and unmarked trace is the measurement inside the AC. Black and unmarked trace is the measurement inside the RC, where the antenna was pointed toward a wall with no stirrer at a distance of about 75 cm. Green and square-marked trace is the mismatch by gating from measurements inside the RC, where the FR is equal to of the AUT. The GA ranges from −2 ns to 2 ns. In order to avoid misunderstandings, it is stressed that the part of measurements outside the FR of the AUT does not correspond to any modal impedance. (b) Mismatch (S_{11}) in TD of the X-Band standard horn antenna. Red and unmarked trace is the measurement inside the AC. Black and cross-marked trace is the measurement outside the AC.

We note that for such a log-periodic antenna, the multiple reflections along the body of the antenna are visible also when the abovementioned windowing is applied, i.e., when $\beta = 6$. Fig. 17(a) and Fig. 17(b) clearly show the multiple reflections along the body of the log-periodic antenna both when the FR of the AUT and Δf are used, respectively. In fact, the coefficient β of the Kiser-Bessel window is put to 6 and 0 in Figs. 17(a) and 17(b), respectively where $\beta = 0$ means that the natural rect function is used. From Fig. 15(c), Fig. 16(c), Fig. 17(a), and Fig. 17(b), we note a small mismatch at calibration plane and the mismatch at the tip of the log-periodic where the array of dipoles is really fed, which is located at 6 ns from the calibration plane. The radio frequency connection of the coaxial

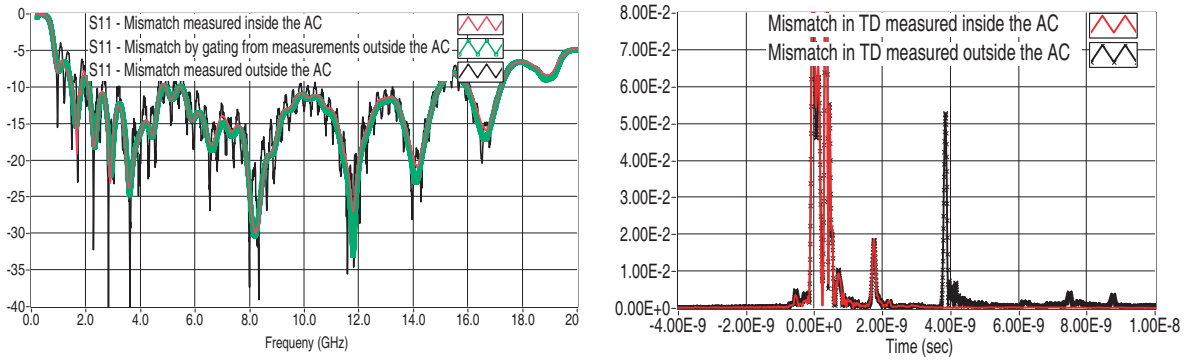

(a) (b)

Figure 10. Mismatch (S_{11}) in dB of the double ridge waveguide horn antenna, model ETS-Lindgren 3115. Red and unmarked trace is the measurement inside the AC. Black and unmarked trace is the measurement outside the AC, where a metallic slab is in front of the antenna at a distance of about 35 cm. Green and square-marked trace is the mismatch by gating from measurements outside the AC. The GA ranges from -2 ns to 2 ns. In order to avoid misunderstandings, it is stressed that the part of measurements outside the FR of the AUT could be not connected to the concept of impedance mismatch. (b) Mismatch (S_{11}) in TD of the double ridge waveguide horn antenna. Red and unmarked trace is the measurement inside the AC. Black and cross-marked trace is the measurement outside the AC.

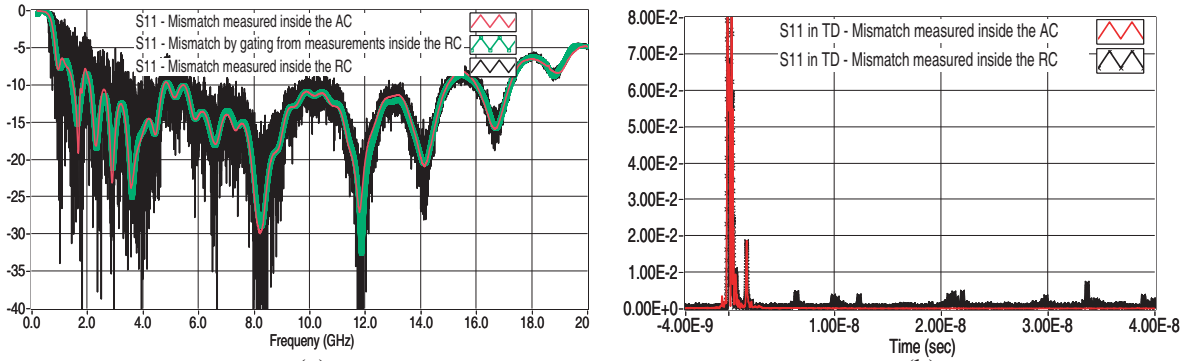

(a) (b)

Figure 11. (a) Mismatch (S_{11}) in dB of the double ridge waveguide horn antenna, model ETS-Lindgren 3115. Red and unmarked trace is the measurement inside the AC. Black and unmarked trace is the measurement inside the RC. Green and square-marked trace is the mismatch by gating from measurements inside the RC. The GA ranges from -2 ns to 2 ns. In order to avoid misunderstandings, it is stressed that the part of measurements outside the FR of the AUT could be not connected to the concept of impedance mismatch. (b) Mismatch (S_{11} in TD) of the of the double ridge waveguide horn antenna. Red and unmarked trace is the TD response concerning S_{11} inside the AC. Black and cross-marked trace is the TD response concerning S_{11} inside the RC; the antenna was obliquely pointed toward a wall with no stirrer at a distance of about 75 cm.

cable to the tip of the antenna along with the same coaxial cable work as a balun as well, as mentioned above. Consequently, the nearest-obstacle distance (d) around the AUT is 15 ns $-$ 6 ns $=$ 9 ns, which corresponds to a distance nearest-obstacle distance of 1.35 m when a GA up to 15 ns is used. But, such a distance is not sufficient as it can be seen in Figs. 15(b), 16(b), and Fig. 17(b). In fact, in this case, the value 6 of the coefficient β of the Kiser-Bessel window affects an easy identification of the correct GA. We see that the multiple reflections, whose effects are located distant from reflection of the tip of the antenna, are important at low frequencies as it is expected. This is also verified by several tests where the GA is gradually increased.

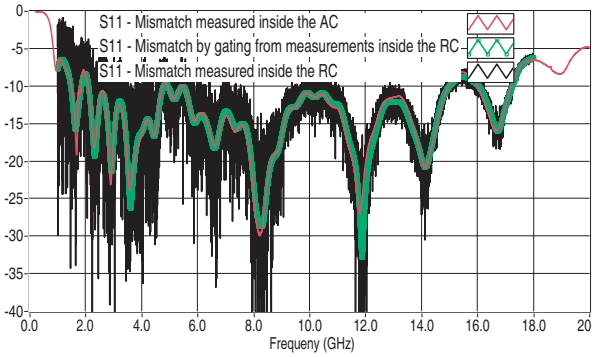

Figure 12. Mismatch (S_{11}) in dB of the double ridge waveguide horn antenna, model ETS-Lindgren 3115. Red and unmarked trace is the measurement inside the AC. Black and unmarked trace is the measurement inside the RC. Green and square-marked trace is the mismatch by gating from measurements inside the RC. The GA ranges from -2 ns to 2 ns. In order to avoid misunderstandings, it is stressed that the part of measurements outside the FR of the AUT could be not connected to the concept of impedance mismatch.

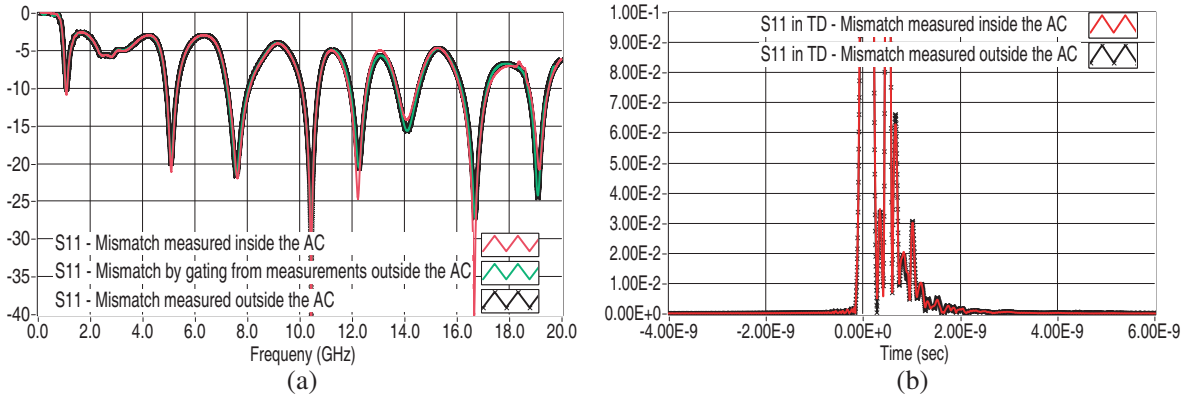

Figure 13. (a) Mismatch (S_{11}) in dB of the homemade sleeve monopole antenna. Red and unmarked trace is the measurement inside the AC. Black and cross-marked trace is the measurement outside the AC. Green and unmarked trace is the mismatch by gating from measurements outside the AC. The GA ranges from -2 ns to 4 ns. In order to avoid misunderstandings, it is stressed that the part of measurements outside the FR of the AUT could be not connected to the concept of antenna impedance mismatch. (b) Mismatch (S_{11}) in TD of the homemade sleeve monopole antenna. Red and unmarked trace is the measurement inside the AC. Black and cross-marked trace is the measurement outside the AC.

It is highlighted that the oscillations at the end of the TD traces in Figs. 15(c), 16(c), and 17(b) are attributed to the non-negligible multiple reflections excited on the body of the AUT at low frequencies, i.e., they are not connected to the leakage in the TD due to the natural rect ($\beta = 0$) in FD. In fact, such oscillations are stronger when Δf is considered as Figs. 17(a) and 17(b) show clearly. In FD, the trace has several oscillations from 250 MHz (f_{MIN}) to 500 MHz as Fig. 15(b) and Fig. 16(b) show. It is found that the mismatch from measurements inside the AC by gating agrees well with the measured mismatch when the selected GA is at least 25 ns, which determines an nearest-obstacle distance of 2.85 m. Such an aperture is necessary to achieve the correct oscillation at low frequencies as well.

It is clear that the method becomes impracticable at low frequencies for log-periodic antennas as Fig. 17(b) also shows; in particular, for the log-periodic tested in this paper, the method becomes impracticable at frequencies less than about 500 MHz. To better understand the usefulness of the frequency measurement extension, we observe that if the f_{MIN} is used as a start frequency, the oscillations distant from reflection of the tip of the antenna reduce, as Figs. 17(a) and 17(b) show. But, when f_{MIN}

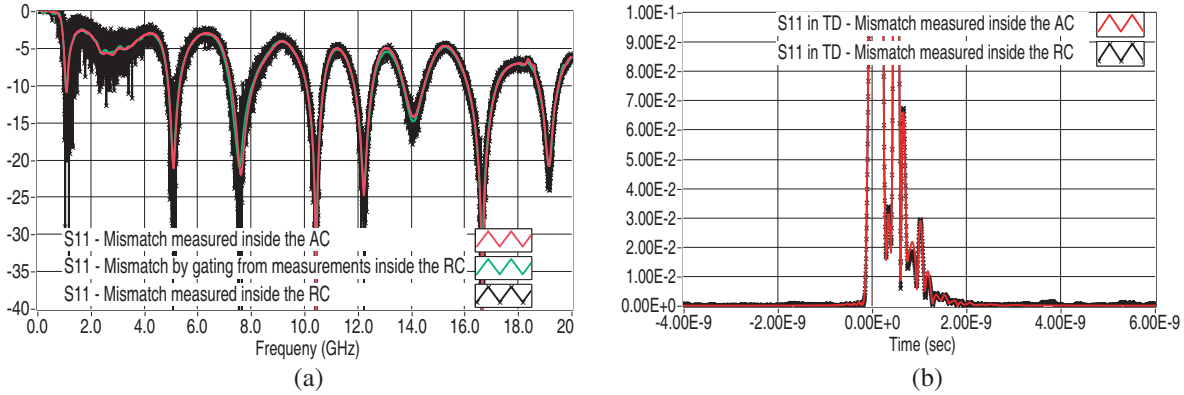

Figure 14. (a) Mismatch (S_{11}) in dB of the homemade sleeve monopole antenna. Red and unmarked trace is the measurement inside the AC. Black and cross-marked trace is the measurement inside the RC. Green and unmarked trace is the mismatch by gating from measurements inside the RC. The GA ranges from -2 ns to 4 ns. In order to avoid misunderstandings, it is stressed that the part of measurements outside the FR of the AUT could be not connected to the concept of antenna impedance mismatch. (b) Mismatch (S_{11}) in TD of the homemade sleeve monopole antenna. Red and unmarked trace is the measurement inside the AC. Black and cross-marked trace is the measurement inside the RC.

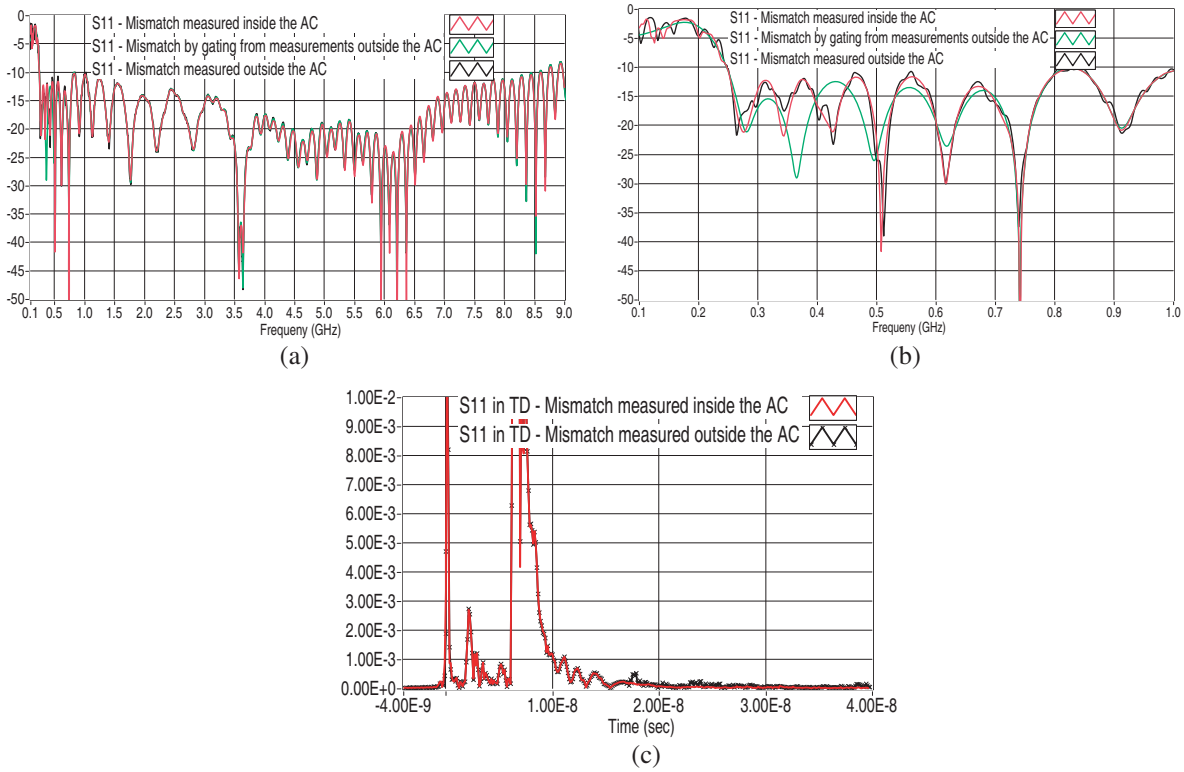

Figure 15. (a) Mismatch (S_{11}) in dB of the log-periodic antenna, model Schwarzbeck Mess — Elektronik USLP-4193. Red and unmarked trace is the measurement inside the AC. Black and unmarked trace is the measurement outside the AC. Green and square-marked trace is the mismatch by gating from measurements outside the AC. The GA ranges from -4 ns to 15 ns. (b) Some details at low frequency of Fig. 16(a). (c) Mismatch (S_{11}) in TD of the log-periodic antenna obtained by off-line data processing. Red and unmarked trace is the measurement inside the AC. Black and cross-marked trace is the measurement outside the AC.

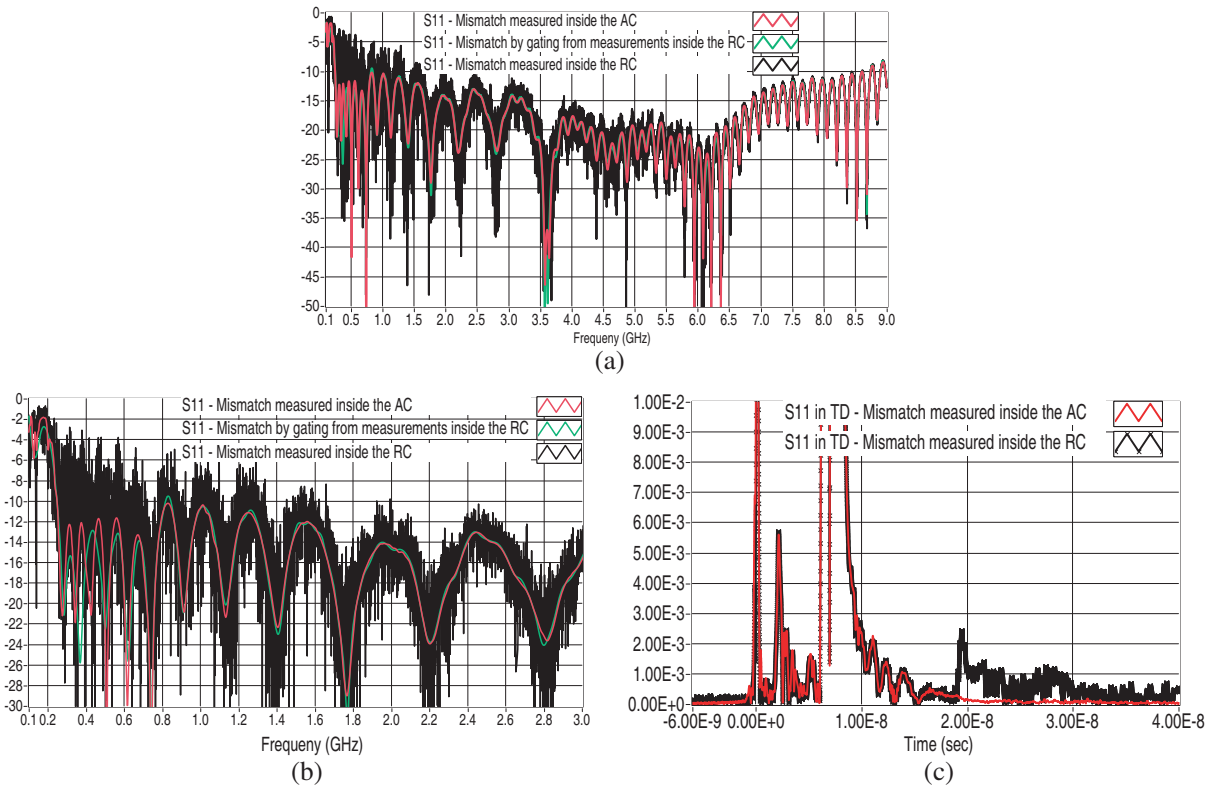

Figure 16. (a) Mismatch (S_{11}) in dB of the log-periodic antenna, model Schwarzbeck Mess — Elektronik USLP-4193. Red and unmarked trace is the measurement inside the AC. Black and unmarked trace is the measurement inside the larger RC. Green and square-marked trace is the mismatch by gating from measurements inside the larger RC. The GA ranges from −4 ns to 15 ns. (b) Some details at low frequency of Fig. 14(a). (c) Mismatch (S_{11}) in TD of the log-periodic antenna. Red and unmarked trace is the measurement inside the AC. Black and cross-marked trace is the measurement inside the larger RC.

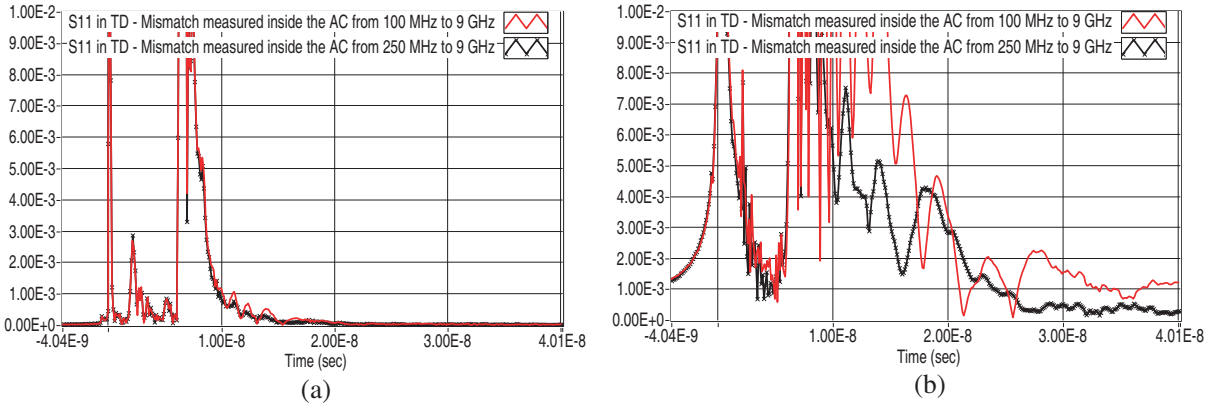

Figure 17. (a) Mismatch (S_{11}) in TD of the log-periodic antenna, model Schwarzbeck Mess — Elektronik USLP-4193 inside the AC; these results are obtained by off-line data processing. The coefficient β of the Kiser-Bessel window is put to 6. Red and unmarked trace is the measurement from 100 MHz to 9 GHz (Δf). Black and unmarked trace is the measurement from 250 MHz, which is equal to f_{MIN}, to 9 GHz. (b) The same as in (a) except for the coefficient β of the Kiser-Bessel window that is put to 0.

is considered as a start frequency, the mismatch from gating shows a considerable truncation problem at edge of the low frequencies, for which the frequency measurement extension is in any case valid. This was clearly verified, even though it is not shown here for the sake of brevity.

5. CONCLUSIONS

It is shown that AIMM of broadband antennas at microwave frequencies can be performed in a generic multipath electromagnetic environment. Measurements are acquired in FD by a VNA in a generic multipath electromagnetic environment, then an IDFT is applied to move into the TD. Finally, a gating operation and a DFT are applied.

The applicability of the method requires a correct GA, which implies the measurement of the AUT reflection response. A minimum distance from the nearest obstacle from the AUT has to be considered in TD response, in order not to affect the intrinsic impedance of the AUT and to correctly measure the GA. The AUT reflection response is achieved by the same measurements for the mismatch of the AUT in a generic multipath electromagnetic environment, where an intentional reflecting obstacle could be used in order to correctly achieve the GA. In this paper, the GA is achieved also by measurements inside the AC in order to validate the proposed approach. Such a method enhances the use of the TD option embedded in VNAs.

Results from measurements carried out inside the AC, outside it, and inside RCs for the X-Band standard horn antenna, the X-Band flanged standard waveguide antenna, the double ridge waveguide horn antenna, the log-periodic antenna, and the homemade sleeve monopole antenna support the practical application of the method proposed in this paper. In particular, the method is powerful for antennas having a short reflection response such as horn antennas. For log-periodic antennas, we found that the method can be applied from frequencies above about 500 MHz.

APPENDIX A.

Sleeve monopole antennas are known in literature [31–40]. They work well in an octave of FR [31]; therefore, under these conditions, a sleeve monopole behaves as a genuine antenna in terms of radiation pattern and mismatch. However, if a moderate mismatch can be accepted for a given application, then such monopoles can be used over a broadband FR [39, 40].

Figure A1 shows the general pattern of a sleeve monopole; the ratio between the lengths L_1 and L_2 fundamentally determines the FR where the sleeve monopole is acceptably impedance matched. However, for the scope of this paper, the FR where a sleeve monopole is acceptably impedance matched is experimentally found by changing the lengths L_1 and L_2.

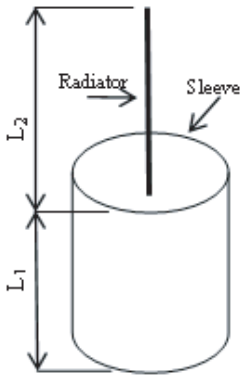

Figure A1. General pattern of a sleeve monopole.

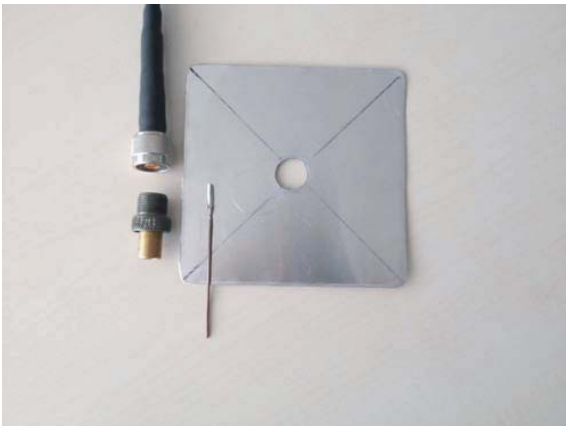

Figure A2. Details for the sleeve monopole concerning the N male connector used for measurements performed in this paper.

The sleeve monopole used for the measurements in this paper is achieved by using N male connectors; however, both connectors, female and male, can be used to achieve the sleeve monopole type shown here. They are made in a very simple way. No dielectric part is integrated to achieve these sleeve monopoles. Details of the sleeve monopole made using an N male connector and used in this paper are shown in Fig. A2; the figure shows the small pipe, wire, and ground plate used to make the sleeve monopole. Note that at one extremity of the wire the small inner sleeve of the N female connector, which matches the wire with the pin of an N male connector, has been soldered. The pipe protrudes out from the edge of the connector for 23 mm and the wire is such that $L_2 = 53$ mm. A ground plane is put at the edge of the connector.

REFERENCES

1. IEEE Std 145-1993, "Definitions of terms for antennas," *IEEE Standards Board*, Jul. 18, 1993, and Sep. 23, 2004.
2. Balanis, C. A., *Antenna Theory: Analysis and Design*, J. Wiley and Sons Ltd., ISBN 0-471-66782-X, 2005.
3. Gifuni, A., "Effects of the correction for impedance mismatch on the measurement uncertainty in a reverberation chamber," *IEEE Trans. Electromagn. Compat.*, Vol. 57, No. 6, 1724–1727, Dec. 2015.
4. Krouka, W., F. Sarrazin, and E. Richalot, "Influence of the reverberation chamber on antenna characterization performances," *Int. Symposium on EMC (EMC EUROPE)*, 329–333, Amsterdam, 2018, doi: 10.1109/EMCEurope.2018.8485064.
5. Carlberg, U., P.-S. Kildal, A. Wolfang, O. Sotoudeh, and C. Orlenius, "Calculated and measured absorption cross sections of lossy objects in reverberation chamber," *IEEE Trans. Electromagn. Compat.*, Vol. 46, No. 2, 146–154, May 2004.
6. Holloway, C. L., H. A. Haider, R. J. Pirkl, W. F. Yong, D. A. Hill, and J. Ladbury, "Reverberation chamber techniques for determining the radiation and total efficiency of antennas," *IEEE Trans. Electromagn. Compat.*, Vol. 60, 1758–1770, Apr. 2012.
7. Ulriksson, B., "Conversion of frequency-domain data to the time domain," *Proc. of the IEEE*, Vol. 74, 74–77, 1986.
8. Papoulis, A., *The Fourier Integral and Its Applications*, Prentice-Hall, New Jersey, 1974.
9. Bracewell, R. M., *The Fourier Transform and Its Applications*, Prentice-Hall, New Jersey, 1974.
10. Bártík, H., "Antenna measurements using the mirror method with gating in a time domain," *Radioengineering Journal*, Vol. 14, No. 4, 58–62, Dec. 2005.
11. Carlson, A. B., *Communication Systems: An Introduction to Signal and Noise in Electrical Communication*, McGraw-Hill, New York, 1986.
12. Brigham, E. O., *The Fast Fourier Transform*, McGraw-Hill, New York, 1986.
13. Wheeler, H., "The radiansphere around a small antenna," *Proceedings of the IRE*, Vol. 47, 1325–1331, Aug. 1959.
14. Agilent Technologies, "Time domain analyzer using a network analyzer," Application note 1287-12, Literature number 5989-5723EN, Published in USA, May 2, 2012.
15. Hiebel, M., *Fundamentals of Vector Network Analysis*, Rhode & Schwarz, München, ISBN 978-3-939837-06-0, 2014.
16. Keysight Technologies, "Time domain analyzer using a network analyzer," Application note 1287-12, Literature number 5989-5723EN, Published in USA, Aug. 2, 2014.
17. Anritsu, "Time domain measurements using network analyzers," Application note No. 11410-00206, Rev. D, Printed in USA, Mar. 2009.
18. Campagnaro, G., "Private communication," Keysight Technologies, Italy, Mar. 2017.
19. Counts, T., A. C. Gurbuz, W. R. Scott, Jr., J. H. McClellan, and K. Kim, "Multistatic ground-penetrating radar experiments," *IEEE Trans. on Geosci. Remote. Sens.*, Vol. 45, 2544–2553, Aug. 2007.

20. Soldovieri, F., O. Lopera, and S. Lambot, "Combination of advanced inversion techniques for an accurate target localization via GPR for demining applications," *IEEE Trans. on Geosci. Remote. Sens.*, Vol. 49, 451–461, Jan. 2011.
21. Peabody, Jr., J. E., G. L. Charvat, J. Goodwin, and M. Tobias, "Through-wall imaging radar," *Lincoln Laboratory Journal*, Vol. 19, No. 1, 2012.
22. Adhyapak, A., Z. Chen, and K. Shimada, "Free-space antenna factor computation using time-domain gating and deconvolution filter for site validation of fully anechoic rooms," *IEEE Trans. Electromagn. Compat.*, Vol. 60, 1045–1052, Aug. 2018.
23. Gifuni, A. and S. Perna, "Analysis on the calculation of the inverse discrete Fourier transform (IDFT) of passband frequency response measurements in terms of lowpass equivalent response," *Progress In Electromagnetics Research*, Vol. 160, 63–69, 2017.
24. Gifuni, A., M. Ambrosanio, G. Grassini, and A. Urciuoli, "Preliminary results on the use of the time domain option in vector network analyzers to measure the impedance mismatch of broadband antennas in any electromagnetic environment," *Fondazione Giorgio Ronchi*, Anno LXXIV, No. 1, 2019.
25. ETS Lindgren, "Antennas," http://www.ets-lindgren.com/products/antennas.
26. A-INFO, "Antennas," http://www.ainfoinc.com/en/p_ant_h.asp.
27. Hemming, L. H., *Electromagnetic Anechoic Chambers*, IEEE Press, Piscataway, NJ, 2002.
28. Corona, P., G. Latmiral, E. Paolini, and L. Piccioli, "Use of a reverberating enclosure for measurements of radiated power in the microwave range," *IEEE Trans. Electromagn. Compat.*, Vol. 18, 54–59, May 1976.
29. Crawford, M. L. and G. H. Koepke, "Design, evaluation, and use of a reverberation chamber for performing electromagnetic susceptibility/vulnerability measurements," *Nat. Inst. Standards Technol. (U.S.)*, Tech Note 1092, Apr. 1986.
30. Ma, M. T. and M. Kanda, "Electromagnetic compatibility and interference metrology," *Nat. Inst. Standards Technol. (U.S.)*, Tech Note 1099, Jul. 1986.
31. Stutzman, W. L. and G. A. Thiele, *Antenna Theory and Design*, 3rd Edition, John Wiley & Sons, Inc., May 2012.
32. Wunsch, A. D., "Fourier series treatment of the sleeve monopole antenna," *IEE Proc. H — Microwaves, Ant. and Prop.*, Vol. 135, 217–225, IET, 1988.
33. Shen, Z. and R. H. MacPhie, "Rigorous evaluation of the input impedance of a sleeve monopole by modal-expansion method," *IEEE Trans. on Ant. and Prop.*, Vol. 44, No. 12, 1584–1591, Dec. 1996.
34. Ning, C. Z., K. Hirasawa, and K. Wu, "A novel top-sleeve monopole in two parallel plates," *IEEE Trans. on Ant. and Prop.*, Vol. 49, 438–443, Mar. 2001.
35. Suh, S.-Y., W. L. Stutzman, and W. A. Davis, "A new ultrawideband printed monopole antenna: The planar inverted cone antenna (PICA)," *IEEE Trans. on Ant. and Prop.*, Vol. 52, No. 5, 1361–1364, May 2004.
36. Bin, Z., Q. Liu, and Y. Ji, "Research on a novel sleeve antenna and its applications," *IEEE International Symposium on Microwave, Antenna, Propagation and EMC Technologies for Wireless Communications*, Vol. 1, 330–333, Beijing, China, 2005.
37. George, T. K., N. Lenin, and M. Sreenivasan, "Wide-band dual sleeve antenna," *IEEE Trans. on Ant. and Prop.*, Vol. 54, 1034–1037, 2006.
38. Dong, T. and Y. Chen, "Novel design of ultra-wideband printed double-sleeve monopole antenna," *Progress In Electromagnetics Research Letters*, Vol. 9, 165–173, 2009.
39. Khan, S. N. and M. A. Ahmed, *Printed Sleeve Monopole Antenna*, Department of Physics, COMSATS Institute of Information Technology, Pakistan, Open Access Publisher, 2011, www.intechopen.com.
40. Huang, P., Q. Guo, Z.-Y. Zhang, Y. Li, and G. Fu, "Design of a wideband sleeve antenna with symmetrical ridges," *Progress In Electromagnetics Research Letters*, Vol. 55, 137–143, 2015.